Design and Testing of Vibration Absorbing

Oceanographic Cable Terminations

by

Ethan L. Butler

Submitted to the Department of
Ocean Engineering in Partial Fulfillment of
the Requirements for the
Degree of

MASTER OF SCIENCE
in Ocean Engineering
at the

Massachusetts Institute of Technology

February 1996

© 1996 Massachusetts Institute of Technology

Signature of Author...............................
Department of Ocean Engineering
November 16, 1995

Certified by.....................................
/
Professor J. Kim Vandiver
Thesis Advisor

Accepted by...
Professor A. Douglas Carmichael
Chairman Department Graduate Committee

DESIGN AND TESTING OF VIBRATION ABSORBING

OCEANOGRAPHIC CABLE TERMINATIONS

by

ETHAN L. BUTLER

Submitted to the Department of Ocean Engineering
on November 15, 1995 in partial fulfillment of the
requirements for the Degree of Master of Science in
Ocean Engineering

ABSTRACT

An experimental study was carried out in an effort to minimize flow induced oceanographic cable vibration. Transverse waves travel along a cable and are reflected at the boundaries creating a standing wave field. A phenomenon known as lock-in occurs when the frequency of these vibrations synchronize with a natural frequency of the cable, resulting in large amplitude vibration. If the vibrations are absorbed rather than reflected at the terminations the wave field is simply translational and lock-in is prohibited, resulting in decreased drag force and vibration amplitude and extended fatigue life.

This investigation employs impedance theory and previously generated governing equations to design mechanical absorbing devices mounted at the cable terminations. These devices were tested both in the laboratory and at sea and underwent several revisions until excellent vibration absorption was achieved. A post experimental analysis suggests possible improvements and alternate materials for the devices in different applications.

Thesis Supervisor: Dr. J. Kim Vandiver

Title: Professor of Ocean Engineering

Background

When long slender cylinders such as ropes or cables are subject to an ocean current, a phenomenon known as vortex-induced vibration (VIV) ensues. The flow is separated and vortices are shed from first one side of the cylinder and then the other in an oscillatory fashion, creating transverse waves that travel along the length of the cable. When such waves encounter a fixed boundary they are reflected, creating standing waves. The synchronization of the standing waves and the vortex shedding process is known as lock-in, which may result in standing waves of large amplitude at the natural frequencies of the cable.

Examples of this standing wave field can be observed in cases as commonplace as the anchor line of a boat moored in a light current. However, this effect presents significant problems to the oceanographic community. When taking measurements in the water column, sensitive instruments are frequently towed on a cable from the stern of a research vessel. Experiments have shown that the drag force on a cable in lock-in is increased by a factor of two or three, making it more difficult to lower an instrument to a desired depth. In addition, generated vibrations may not only interfere with data precision, but also cause fatigue in couplings and in extreme cases put the entire apparatus at risk.

Li's predictions

Professor J. Kim Vandiver and Dr. Li Li of the Massachusetts Institute of Technology have examined the theory behind this problem in great detail. Their proposed solution was to attempt to absorb the waves at the terminations rather than reflect them. While this will not prevent VIV from occurring or completely eliminate vibration in the cable, it will theoretically eliminate standing waves and therefore lock-in.

The frequency of VIV generated vibrations in the cable are governed approximately by the following equation

$$f = \frac{V_n S_t}{d} \tag{1}$$

1

where V_n is the fluid velocity normal to the cable, S_t is the Strouhal number of the cable, and d is the cable diameter. The natural frequencies (in Hz) of a constant tension cable with fixed ends are dictated by

$$f_n = \frac{n}{2L}\sqrt{\frac{T}{\rho_c}} \qquad (2)$$

where T is the cable tension, ρ_c is the linear density of the cable, n is the mode number and L is the cable length.

The parameters of the wave absorbing terminations were defined using impedance theory. If the impedance of the termination were matched to that of an infinite cable, all incident vibration would be absorbed. The termination input impedance Z_m is complex, and is expressed by the following equation.

$$Z_m = \frac{force}{velocity} = R_m + iX_m \qquad (3)$$

The mechanical impedance at the end of a semi infinite cable is real and equal to $\rho_c C$ where C is the wave speed. Therefore, to match the termination to the cable impedance, X_m must equal zero and R_m must equal $\rho_c C$.

equations and graphs

An example of a general termination is shown in Figure 1. The cable ends in a rigid link that is pinned to a fixed object. At point "a" along the link a spring is attached, and at point "b" a dashpot is attached. The equation of motion for such an apparatus is

$$I\ddot{\theta} + R_x b^2 \dot{\theta} + \left(K_x a^2 + TL_L\right)\theta = 0 \qquad (4)$$

where I is the mass moment of inertia of the rigid link about the hinge, R_x is the damping constant, K_x is the spring constant, "a" is the distance from the pivot to the spring, "b" is the distance from the pivot to the dashpot, L_L is the length of the link, and θ is the angle of rotation of the link. The impedance of the termination can then be expressed as

2

$$Z_m = \frac{1}{L_L^2}\left[R_x b^2 + i \frac{-TL_L - K_x a^2 + \omega^2 I}{\omega} \right]$$ (5)

where ω is the frequency of vibration in radians per second. As seen from Equation 3, the imaginary part of this equation must be zero to perfectly match impedances. Therefore Ω, the frequency for which the termination is optimally tuned, and the real part of the termination input impedance, R_m, can be expressed as

$$\Omega = \sqrt{\frac{TL_L + K_x a^2}{I}}$$ (6)

and

$$R_m = \frac{b^2}{L_L^2} R_x = \rho_c C$$ (7)

These are the two definitive equations that must be satisfied by the terminations for total absorption.
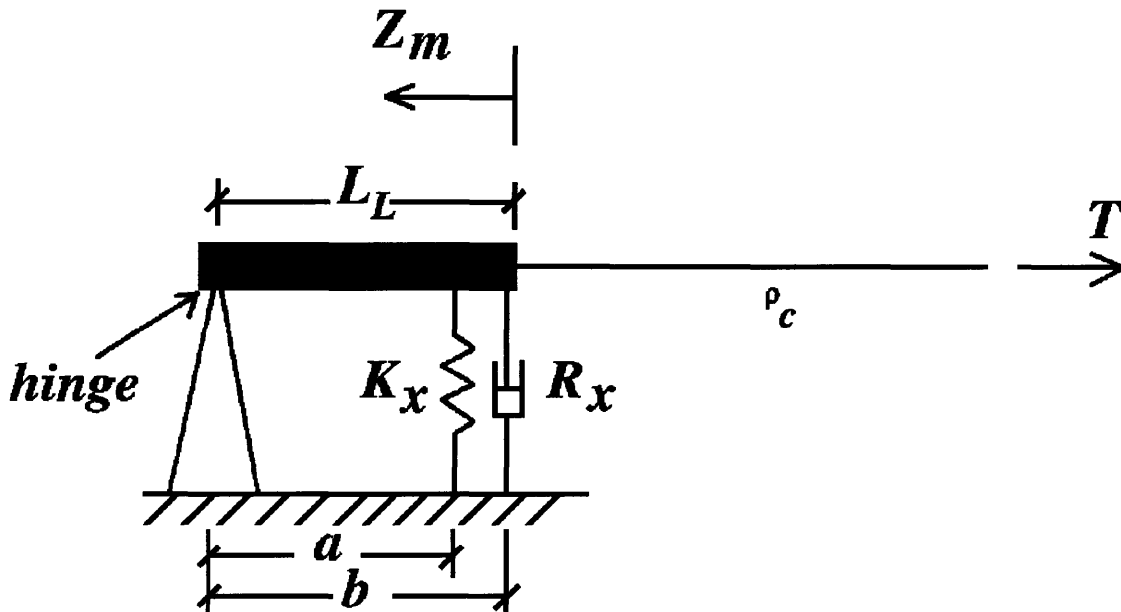

Figure 1: A general termination

Dr. Li and Professor Vandiver have evaluated such a termination's performance under other than optimized conditions, and a prediction of these

3

results is shown in Figure 2. The power absorption ratio α was defined to be unity at total absorption and zero at no absorption, and is expressed as

$$\alpha = \frac{4R_r}{\left(1+R_r\right)^2 + R_d^2\left(\overline{\omega} - \frac{1}{\overline{\omega}}\right)^2} \qquad (8)$$

where $R_r = \dfrac{Rb^2}{\rho_c C \, L_L{}^2}$, the ratio of the device resistance to the ideal resistance;

$R_d = \dfrac{I\Omega}{\rho_c C \, L_L{}^2}$, a parameter characterizing the useful bandwidth of the power

absorption curve; and $\overline{\omega} = \dfrac{\omega}{\Omega}$, a dimensionless frequency. At values of $\overline{\omega}$

greater or less than unity, power absorption decreases considerably. It should be noted, however, that this decrease is more pronounced for values less than unity.
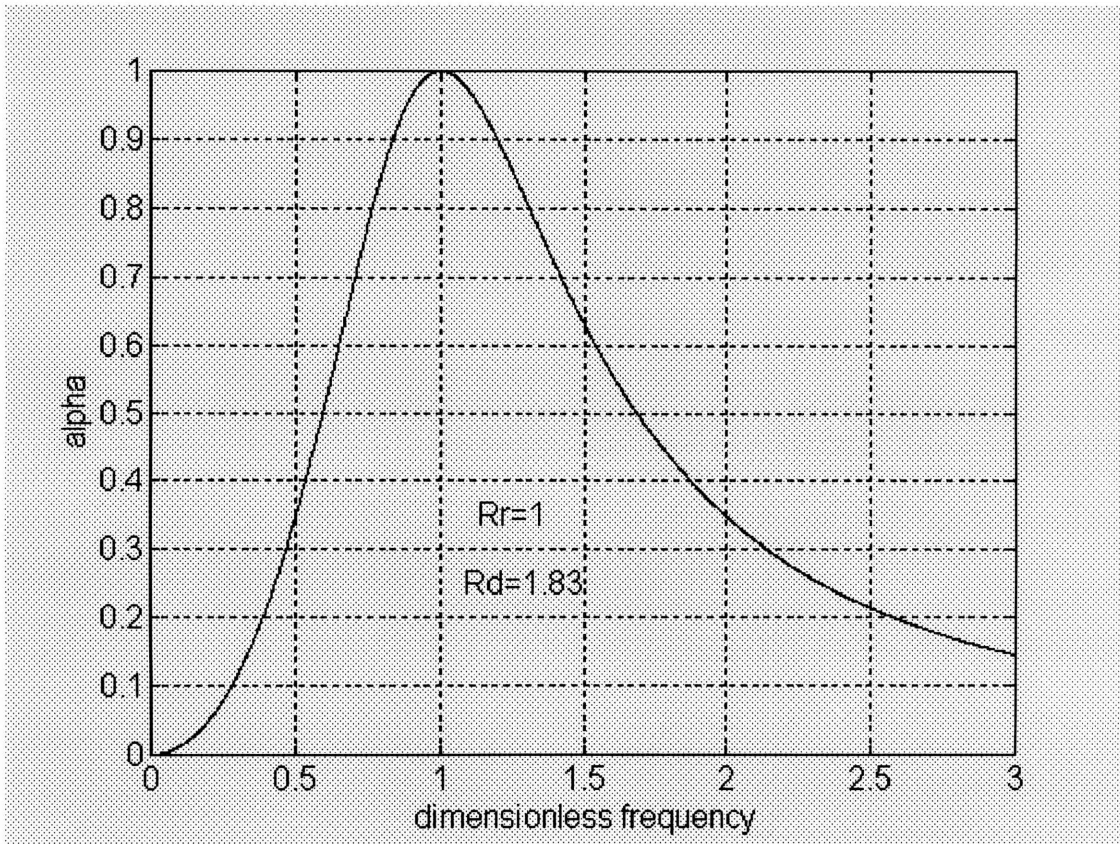
Figure 2: Predicted absorption

conversion from linear to rotational equations

Unfortunately, this linearly damped model requires a fixed platform to which the spring and dashpot may be attached. To simplify design and conform to existing towing hardware, it was decided for this project to use a rotational damper at the hinge and to eliminate the spring altogether. A rotational damper mounted at the hinge with damping constant R_θ can be compared to the effect of a linear damper with damping constant R_x mounted at a distance b from the hinge as

$$R_\theta = R_x b^2 \tag{9}$$

final equations as basis for design

As a result, the final equations used in the design of these terminations were

$$K_\theta = 0 \tag{10}$$

$$I\ddot{\theta} + R_\theta \dot{\theta} + \left(TL_L\right)\theta = 0 \tag{11}$$

$$\Omega = \sqrt{\frac{TL_L}{I}} \tag{12}$$

$$R_m = \frac{R_\theta}{L_L{}^2} = \rho_c C = \sqrt{T\rho_c} \tag{13}$$
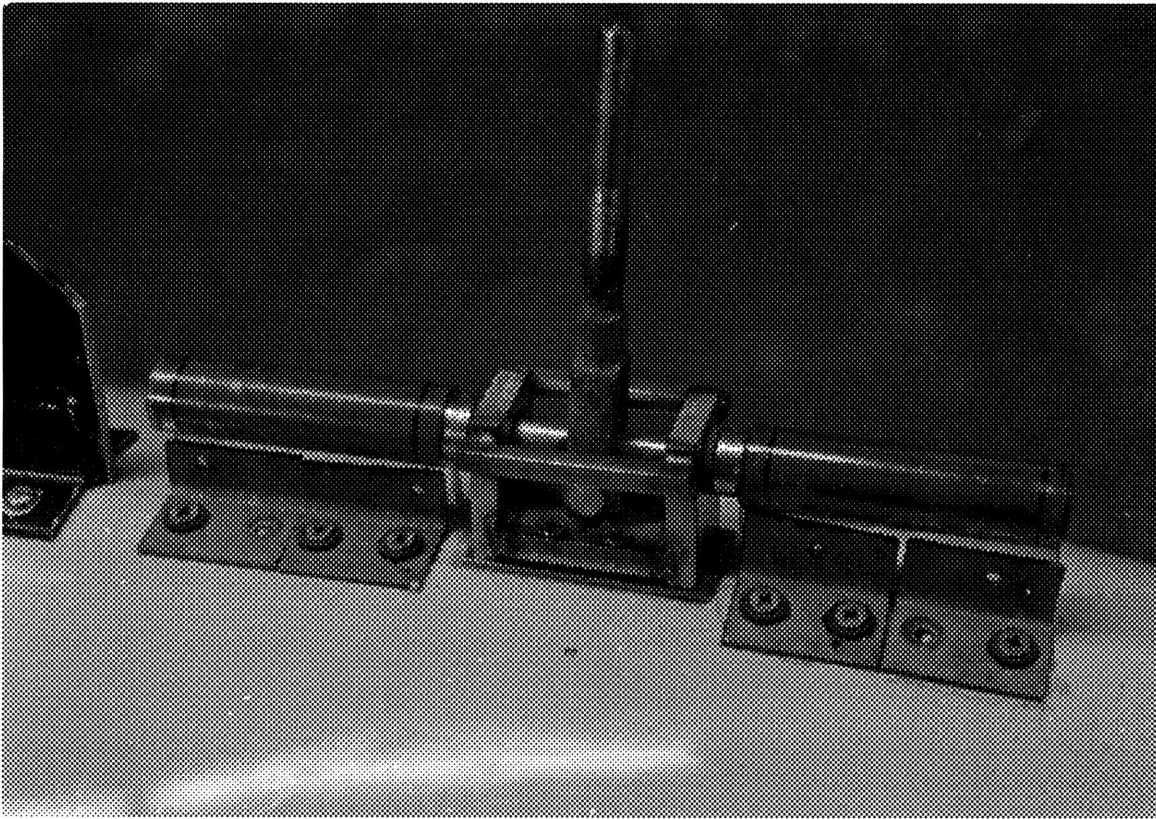
Design

The first consideration in any oceanographic design project is materials. The ocean is an extremely hostile environment for metals, but most applications require their strength. Stainless steel is one of the most stable metals in seawater, and it was exclusively used for all metal parts to minimize the chance of cathodic deterioration. Teflon and Teflon impregnated plastics were used in all cases where friction was to be minimized such as in bushings and washers. Neoprene o-rings were also utilized.

In an effort to maintain simplicity, it was decided that both top and bottom terminations be of the same design. A V-fin depressor wing shown in Figure 3 was used in sea tests at the lower end to introduce tension in the cable. The termination baseplates were designed to fit the existing attachments on the wing. Since a rotational damper was decided upon, cable vibration needed to be transferred from the rigid link to shaft rotation. This meant bearing blocks and bushings were needed to support the shaft and eliminate free play. The rotational dampers were attached to both ends of the shaft to reduce the oscillatory vibration. Figure 4 shows a photo of the termination at this point.
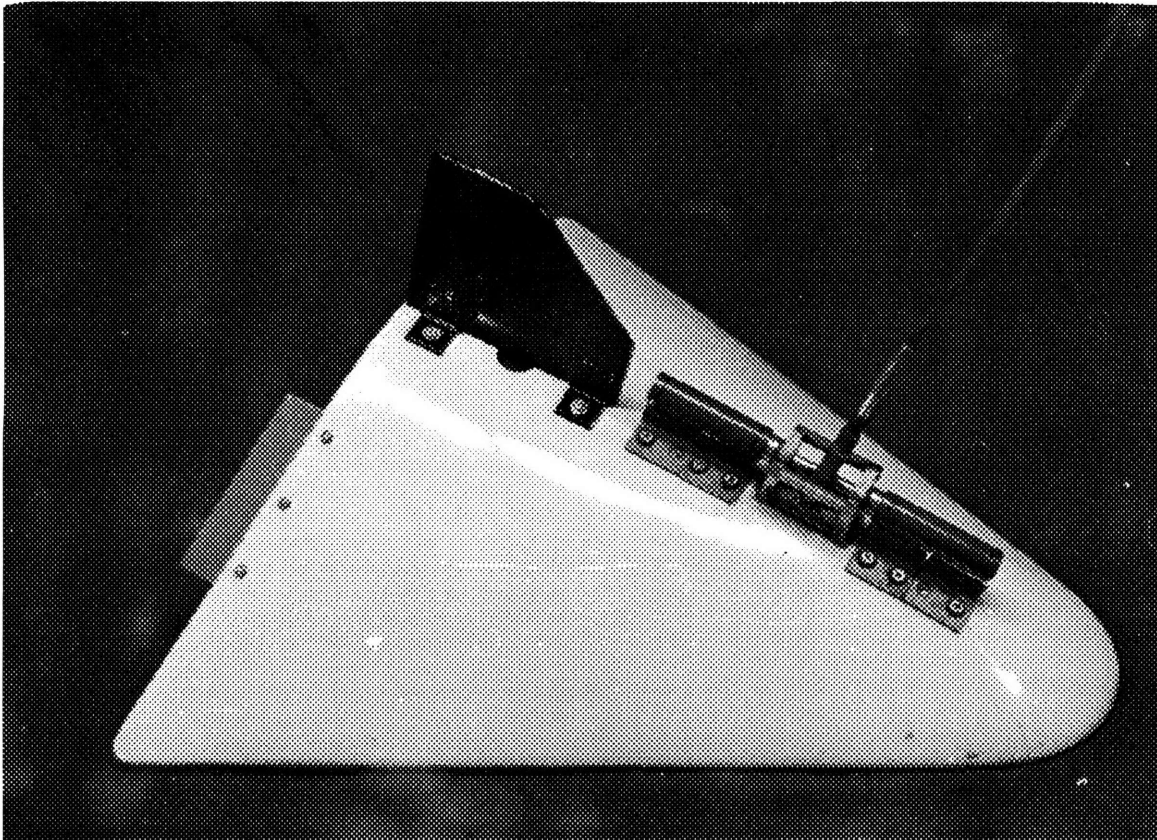
Figure 3: V-fin depressor wing

Figure 4: Termination with no scope angle

Facts of oceanographic instrument towing also determined part of the design. Since drag force on the cable and downward lift on the V-fin are proportional to boat speed squared, the angle the cable makes with the water (scope angle) changes as well. The apparatus needed to be tested at several boat speeds, so it had to have enough freedom to permit this change in angle without sacrificing performance or requiring tedious adjustments. Therefore, the connection point between the link and shaft needed to be free to adjust in pitch angle to allow for different scope angles, but be rigid in the roll direction to transfer cable vibration to the shaft. (See Figure 5.) The simplest solution to this problem was to have the rigid link end in a pinned fork, weld a block to the underside of the shaft, and bore a hole through the block to tightly accommodate the fork pin. It also made it necessary to place shaft collars on the axle to prevent it from slipping fore and aft. Figure 6 illustrates these changes.
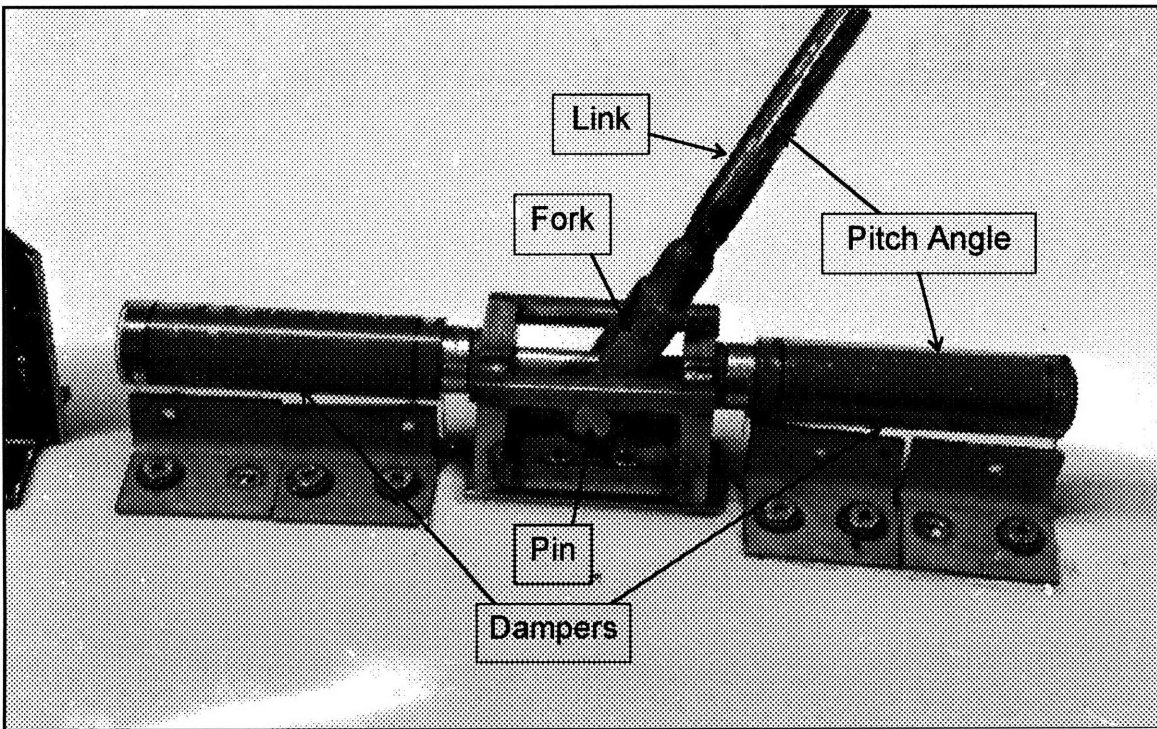
7

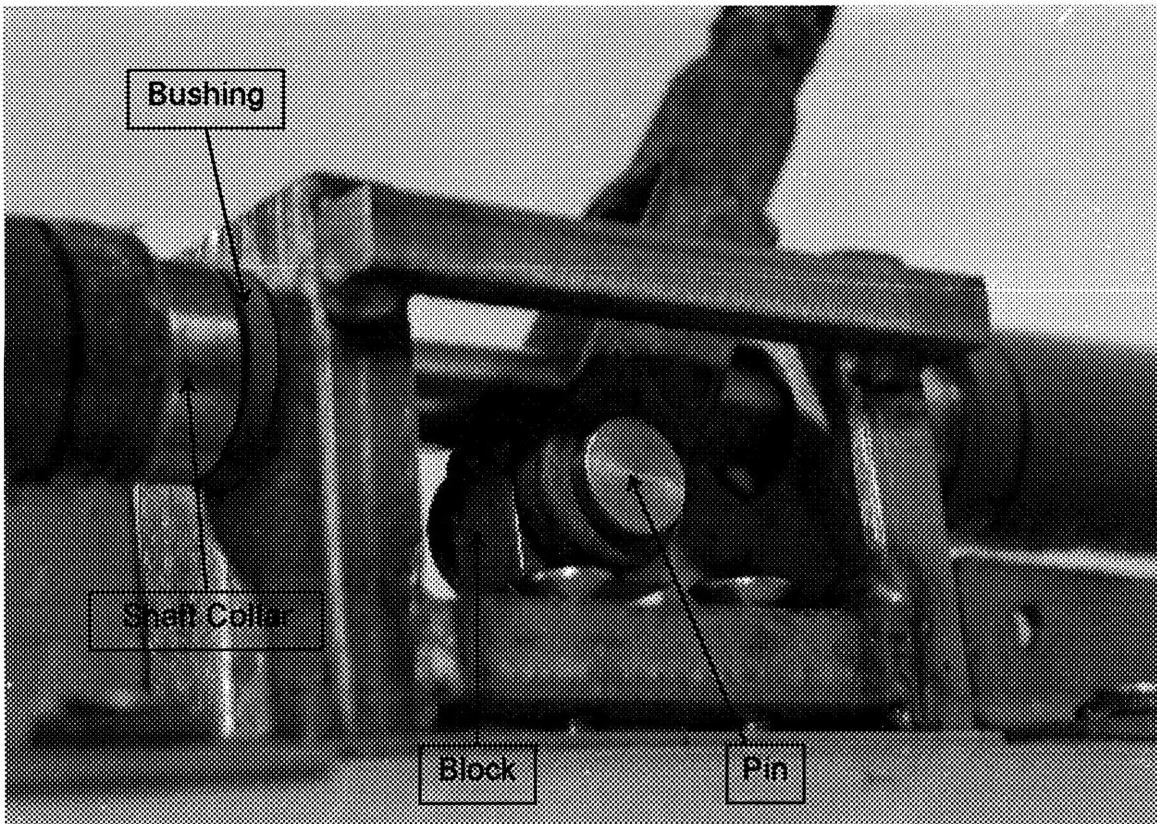**Figure 5: Termination allowing approx. 60° scope angle**

Figure 6: Close-up of pinned fork attachment

The stainless steel cable for the experiment was chosen for its weight in conjunction with its large diameter of .323 inches and therefore low vortex shedding frequency. Three sixty foot lengths of the cable were taken to a marine supply store and 1/2 inch male threaded fittings were swaged onto the ends. These male threads were not used. Holes were drilled and tapped into the ends of these fittings, and 5/16 inch threaded rods were inserted. The pinned forks had 5/16 inch threaded sockets which were screwed onto the exposed ends of these rods. Finally, all junctions were welded.

The next step in designing the terminations was to develop a rotational damper that supplied sufficient energy absorption. The best approach seemed to be a viscous fluid or gel sheared in the space between two concentric sleeves. Eric Marsh of the Massachusetts Institute of Technology worked with such fluids in a constrained layer damping scenario during his doctoral work to minimize vibration in machine tools.

Eric's information on fluids

Dr. Marsh tested two commercial silicone fluids to determine their viscosity as a function of frequency. His viscometer was a linear device that sheared the fluid between two flat plates. Figure 7 shows the viscosity of Dow Corning Viscasil 600,000 and Nusil Corporation's 2.5M centistoke fluid. The resulting curve fit is correct for both fluids above 10 Hz and gives the viscosity in kg/(m·sec).
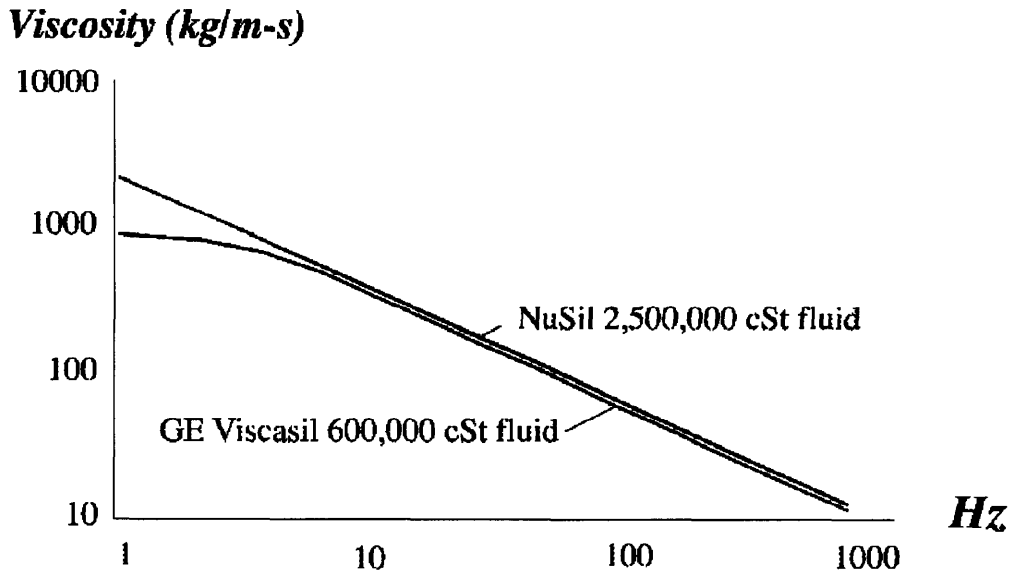
Viscosity (kg/m-s)

Figure 7: Frequency dependance of fluid viscosities

$$\mu(f) = 1300 f [Hz]^{-0.72} \quad \text{in kg/(m·sec)} \qquad (14)$$

Instructions are also given in Dr. Marsh's thesis for designing a linear damper with these fluids. He mentions that a gap of .005 inches between the two plates provided for the maximum shear on the fluid, and therefore maximum damping per area, without undue risk of binding.

Configuring this fluid into a rotational damper was a more difficult task. An equation taken from Mechanical Vibration by Singiresu Rao relates the physical properties and geometry of a torsional damper to the damping constant. The dimensions of this textbook damper are illustrated in Figure 8, and the damping constant is defined as

$$R_\theta = \frac{2\pi\mu R_D^3 L_D}{h} + \frac{\pi\mu R_D^4}{4D} \qquad (15)$$

However, the damper in the figure was slightly different from the planned design. The task remained to develop a new equation for the prototype from this example. While Figure 8 shows a piston rotating in a pot of fluid, the planned damper was to be a pipe surrounded by a collar with fluid in the gap. (See Figure 9.) The damping contribution of the sides of the piston are valid, but the

10

interaction between the bottom of the piston and the pot bottom in the textbook case does not apply. The variable D in equation 15 may be assumed to be infinity, and the entire second term on the right hand side of the equation therefore goes to zero. This leaves a much simpler equation

$$R_\theta = \frac{2\pi\mu R_D^3 L_D}{h} = L_L^{\ 2}\sqrt{T\rho_c} \qquad (16)$$
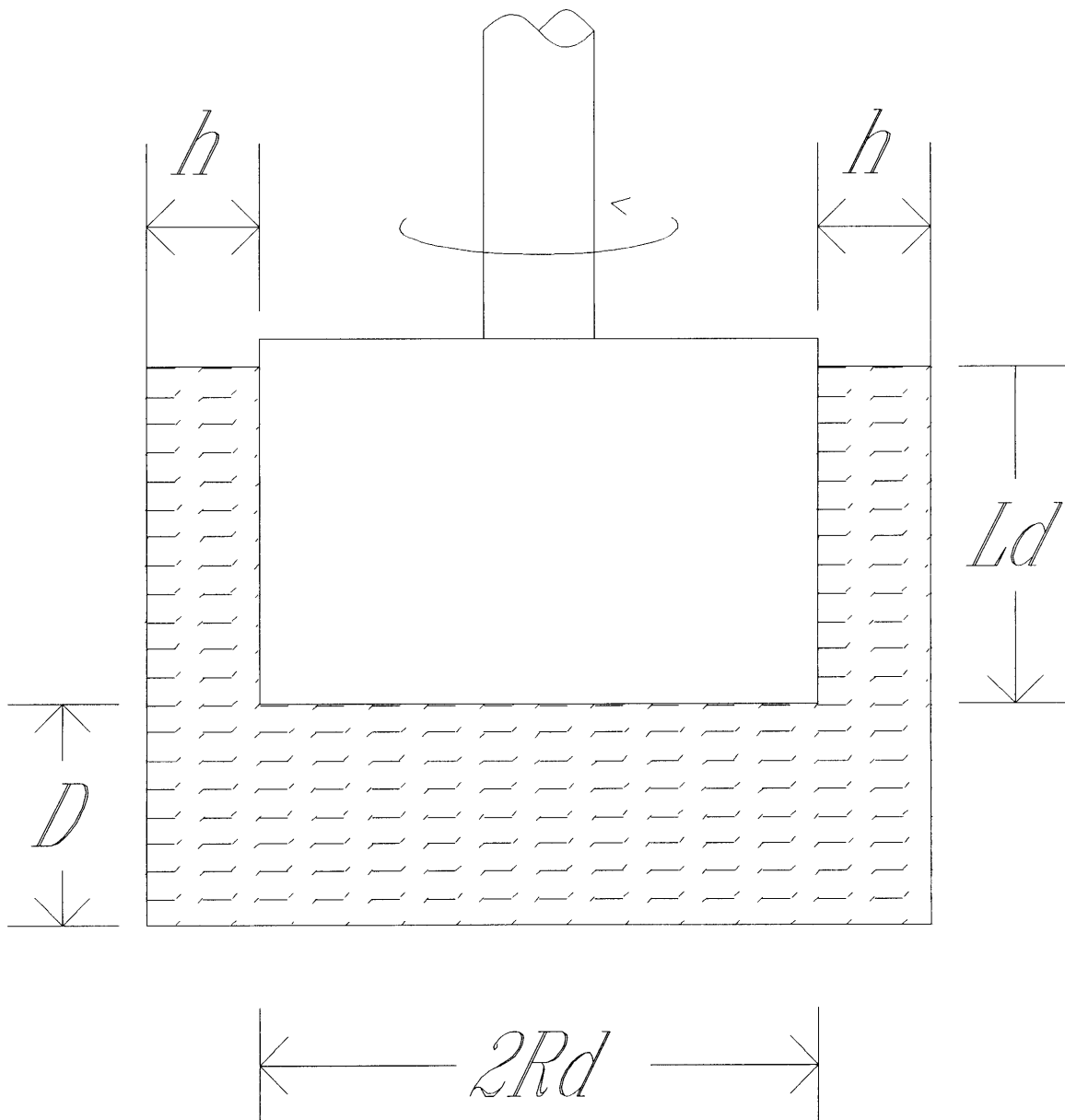
Figure 8: Textbook representation of rotational damper
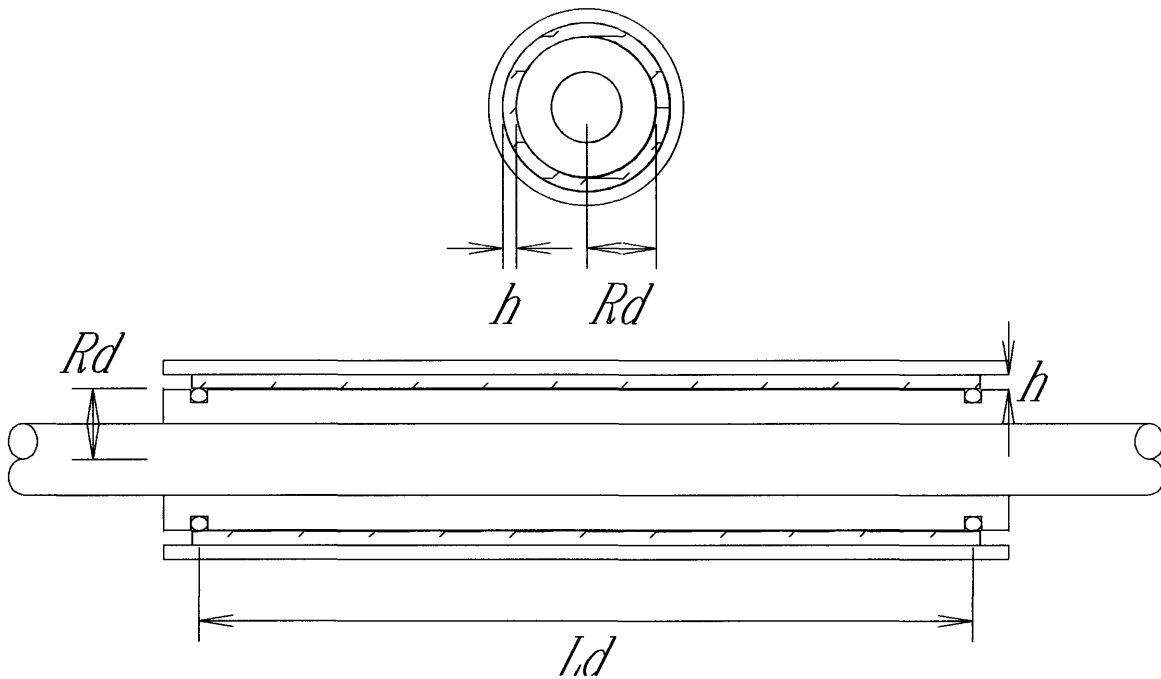
Figure 9: Example of designed damper (gap enlarged for clarity)

A range of useful rotational damping constants was constructed by solving Equation 13 using the measured values of link length L_L and cable mass per unit length ρ_C as well as predictions provided by Mr. Ted Brainard for cable tension T at realistic towing speeds. The generated vibration frequencies corresponding to these towing speeds were determined by assuming a Strouhal number of .17 and solving f = St V/d (Equation 1) using the established cable diameter d = .323 inches. Subsequent solution of equations 14 and 16 using Dr. Marsh's ideal .005 inch gap for h showed that it was theoretically possible to construct dampers for corresponding boat speeds up to 10 knots.

Prototype dampers optimized for 6 knots were built with an outer sleeve of stainless steel pipe and an inner sleeve of sintered bronze tubing turned down on a lathe to provide the correct fluid thickness. This inner sleeve was attached to the axle of the termination with two set screws for easy removal and possible substitution of another damper assembly during sea testing. The gap was sealed with o-rings, fluid was liberally applied, and the outer sleeve was slid into place and secured to a fixed surface as detailed in Figure 10. The friction of the

12

o-rings was not accounted for in the damper design, but the effects were considered negligible.

However, at initial sea trials in August 1994, the dampers did not perform as expected. After disassembly, it was discovered that the set screws through the bronze inner sleeves had gouged into the bronze almost immediately and allowed a critical amount of free play in the system. It was reasoned that the set screws were taking the entire torsional load and concentrating it at two points in the soft bronze. It was decided therefore to sacrifice exchangeability of the dampers and fuse the second generation of damper inner sleeves to the axle. The new inner sleeves were constructed from gray PVC rod and glued to the shaft. Another design modification for the next series of dampers was to use clear plastic for the outer sleeve to allow examination of the dampers in action.
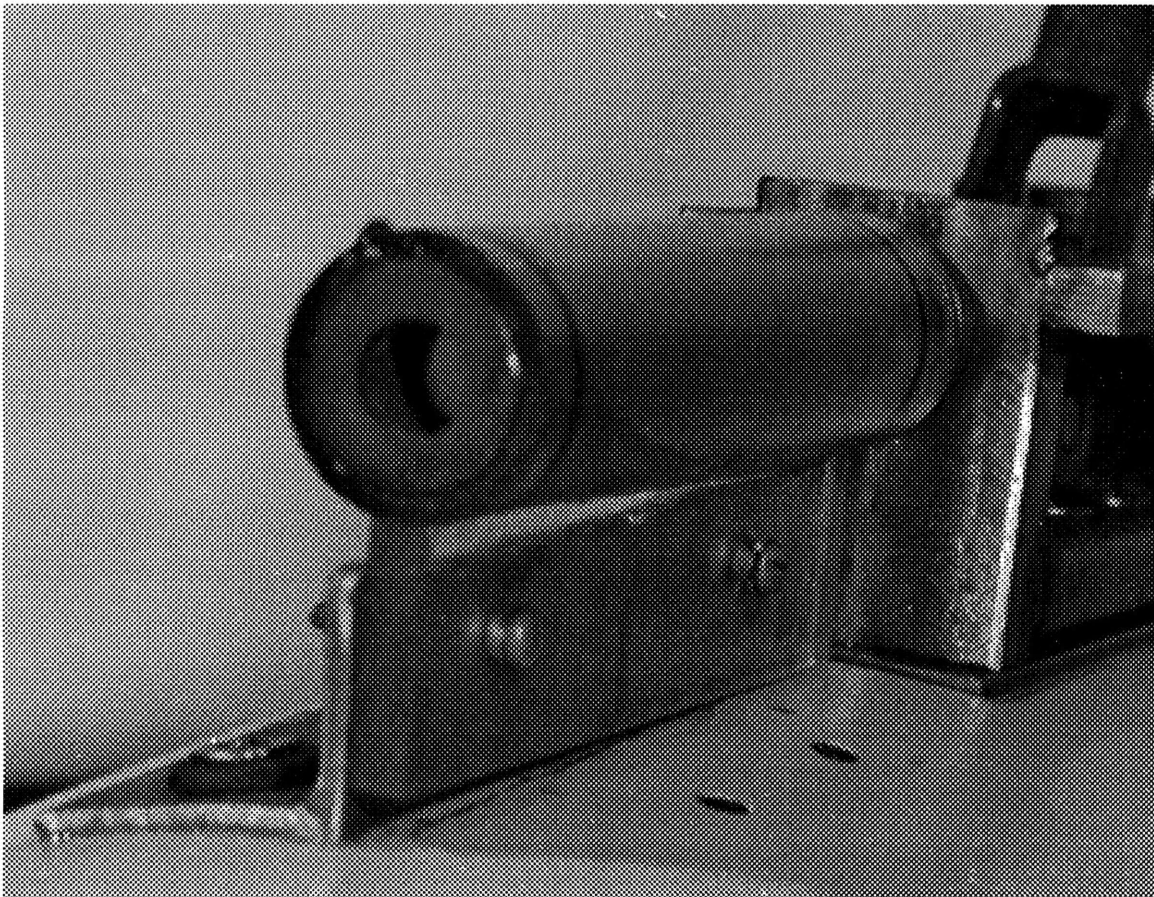
**Figure 10: Close-up of the final damper outer sleeve attachment**

Measurements

A termination fitted with second generation dampers was mounted on a vibration isolating bench and a large electrodynamic shaker was used to excite the assembly. A pushrod was attached to the shaker head, and an impedance head was attached to the end of the pushrod. The impedance head was initially glued to the sample link, but at realistic vibration amplitudes the glue cracked. To remedy this problem, a hemispherical glass bead was glued to the impedance head and a corresponding cavity was drilled into the link, forming a ball and socket joint. Free play was eliminated by pre-loading the ball and socket with a hose clamp. This test setup is illustrated in Figure 11.
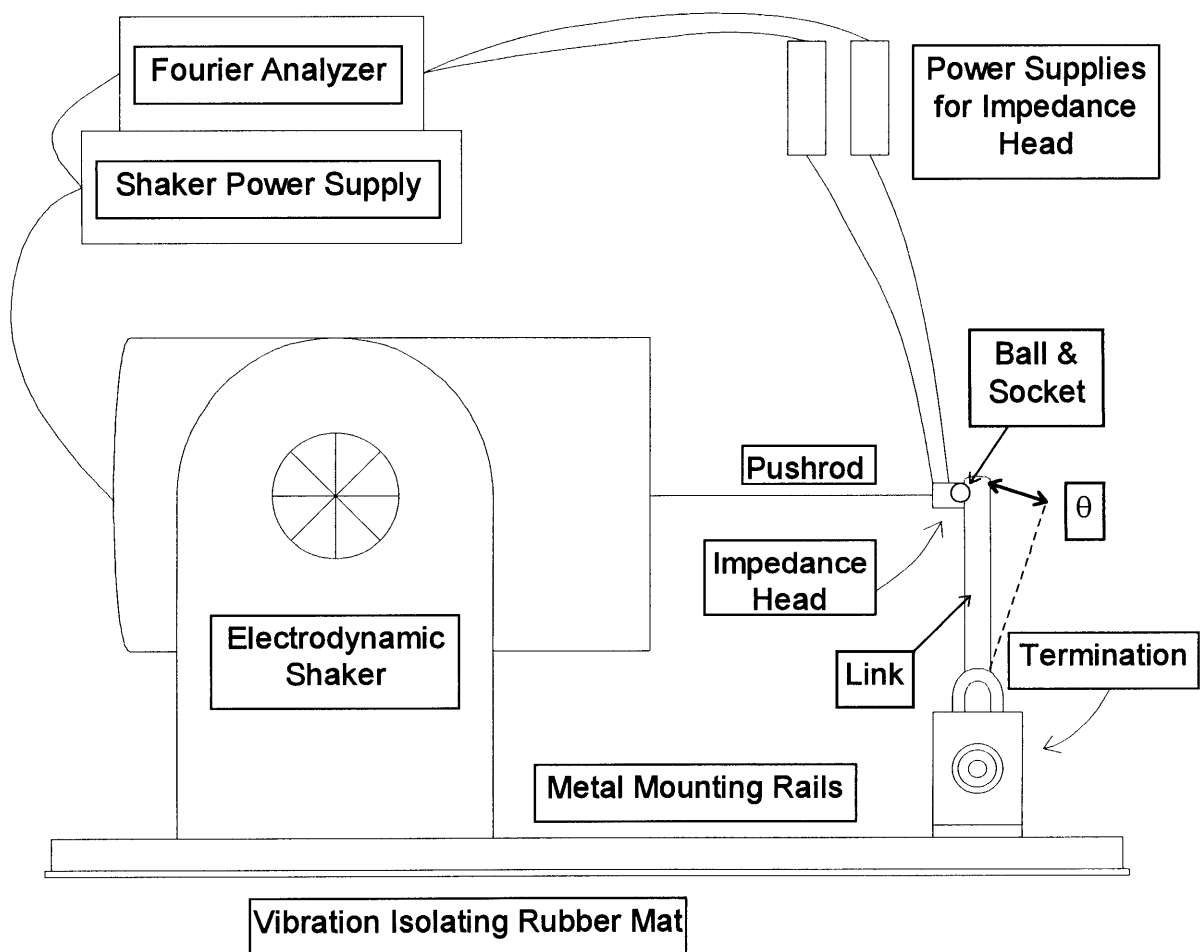
Figure 11: Laboratory test bench setup

14

Although there was no free play between the axle and the new inner sleeves, analysis of the measured force versus acceleration transfer function taken at the end of the link indicated a marked difference between theoretical and experimental performance. Examination of the dampers during testing revealed that unanticipated bubbles had appeared in the fluid, evidently altering the damping of the apparatus significantly. These bubbles are clearly seen in Figure 12.
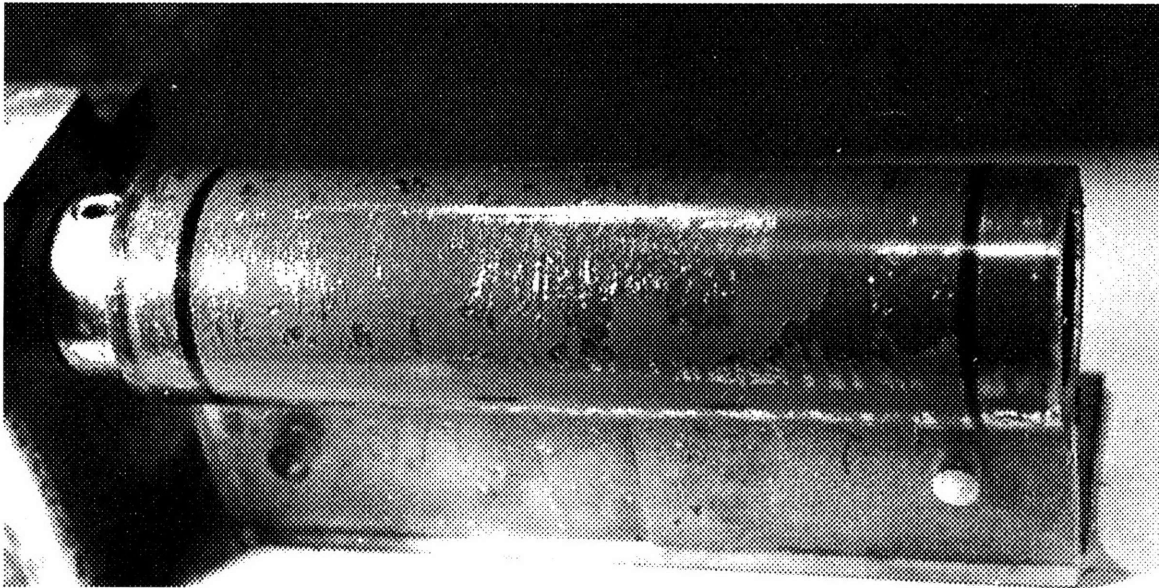
Figure 12: Close-up of bubbles in fluid

Testing results of fluid and design modifications

Several theories explained the existence of the bubbles. It was possible that in the process of filling and assembling the dampers, air bubbles were entrained in the fluid. It was also conceivable that certain volatile components were coming out of solution when the fluid was sheared. Additionally, fluid may have been leaking out through the o-ring seals.

The Nusil company confirmed that their fluid was known to outgas under certain low pressure conditions, so a sample was placed in a vacuum chamber and allowed to boil until the bubbles ceased. The fluid did outgas considerably, and did not repeat under subsequent vacuum treatments. However, when some

of the degassed sample was placed in the dampers the bubbles were still present.

The assembly was then vibrated for an extended period of time to determine if leakage was the problem. At the conclusion of the test it was not evident that any significant amount of the fluid had escaped. It was therefore decided that the bubbles were a product of damper assembly, but no easy solutions presented themselves, even with prior vacuum treatment of the fluid.

Tests were then performed to determine the repeatability of the change in damper performance due to the bubbles. Fortunately, each time the dampers were filled and a test was performed, the resulting damping properties were almost exactly the same. It was therefore decided that eliminating the bubbles from the dampers was beyond the scope of this project, and that damper properties with bubbles would be used.

A new variable called effective viscosity μ_{eff} was created to describe the viscosity of a fluid containing bubbles and bounded by o-rings. It was substituted into equation 16 for Dr. Marsh's expression for viscosity μ, and its value was determined by evaluating damper test results. An example of such a test result is shown in Figure 13. A curve fit was established for the damping constant, and by substituting the appropriate damper geometry values into equation 16, μ_{eff} was defined as

$$\mu_{eff} = 8366 f[Hz]^{-1.4} \tag{17}$$

Thus the proven constant equation used in the third and final generation was obtained by substituting Equation 17 into Equation 16 and modifying for two dampers.

$$R_\theta = \frac{16732\pi f[Hz]^{-1.4} R_D^3 (2L_D)}{h} \quad \text{in} \quad \frac{N \cdot m \cdot \sec}{rad} \tag{18}$$

The device was optimally tuned to a frequency of 53.8 Hertz, corresponding to a cable tension of 350 pounds, known to be present at a boat speed of

16

approximately 5.8 knots. The dampers each had a length L_D of 11.8 cm, a gap h of .005 inches, and a radius R_D of 1.27 cm.
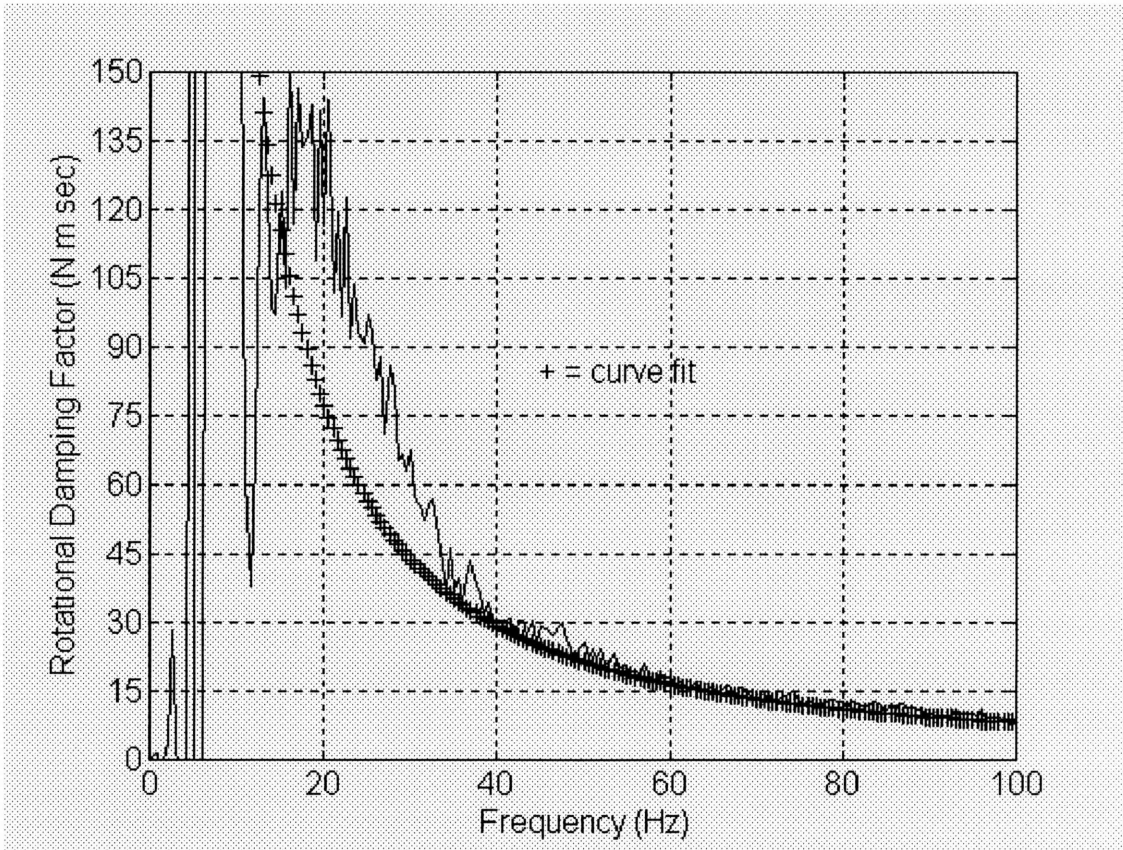

Figure 13: Experimental damping results and curve fit definition of effective viscosity

Before another foray to sea, it was decided to test the entire cable outfit in a realistic scenario. It seemed the most convenient course to hang the cable, terminations and V-fin in a stairway high enough to accommodate all 60+ feet. A brace was built at the top end to support the assembly and serve as an attachment point for the upper termination. The V-fin was attached at the bottom of the cable.

This simulation of at-sea conditions did pose several problems. There was no lift or drag on the V-fin, making it less stable. The tension in the cable was also based simply on the weight of the components. According to Equations 12 and 13, both the optimum frequency and the required damping go

as the square root of tension. Fortunately, the tension in the cable was at almost exactly one fourth its expected at-sea value. The optimum frequency and required damping were therefore halved in the stairway. To adjust the damping, initially only one of the two dampers on each termination was attached.

Accelerometers were glued to the setup at the end of the top link, at the midpoint, and on the fin at the bottom. Since Dr. Li's analysis is geared toward the absorption of a given pulse, the assembly was given impulse excitation with a soft tip force hammer and the time histories of the accelerometers were analyzed. An example of the input spectrum from this hammer is shown in Figure 14.
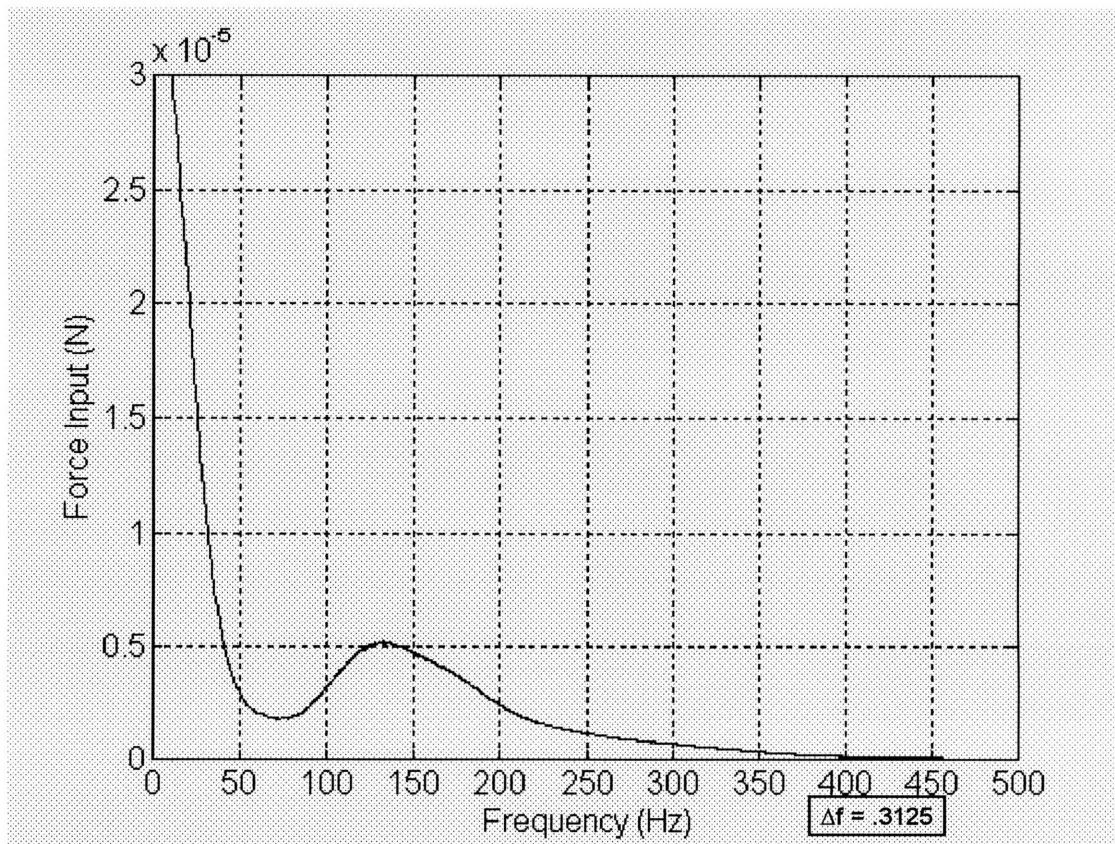
Figure 14: Force hammer input spectrum

Data from these experiments is plotted in Figures 15, 16, and 17. There is a transverse wave that travels from point A at the top of the apparatus, to point B at the midpoint, to point C at the wing, to point D back at the midpoint, to point

E back at the top, and to point F at the midpoint again. There is another axial pulse that travels much faster. It leaves point A the same time as the transverse wave, but reaches the midpoint of the cable at B', and finds the bottom at C'. Ripples in the acceleration of the top link are a result of subsequent arrivals of this axial pulse. It can be seen throughout the graph since there is very little axial damping.

However, results from these tests were far from conclusive. As shown in Figure 14, the amount of energy it was possible to input to the system with the force hammer was small compared to the energy input at sea. Consequently, the links moved very little and the apparent damping with and without dampers seemed about te same. This effect is illustrated by comparing the motion of the top link in Figure 15 (with no dampers attached) to those in the previous Figures 16 (with one damper) and 17 (with both dampers attached at each termination). The fact that there is a reduction in acceleration in the undamped case suggests that there is significant damping in the cable itself.
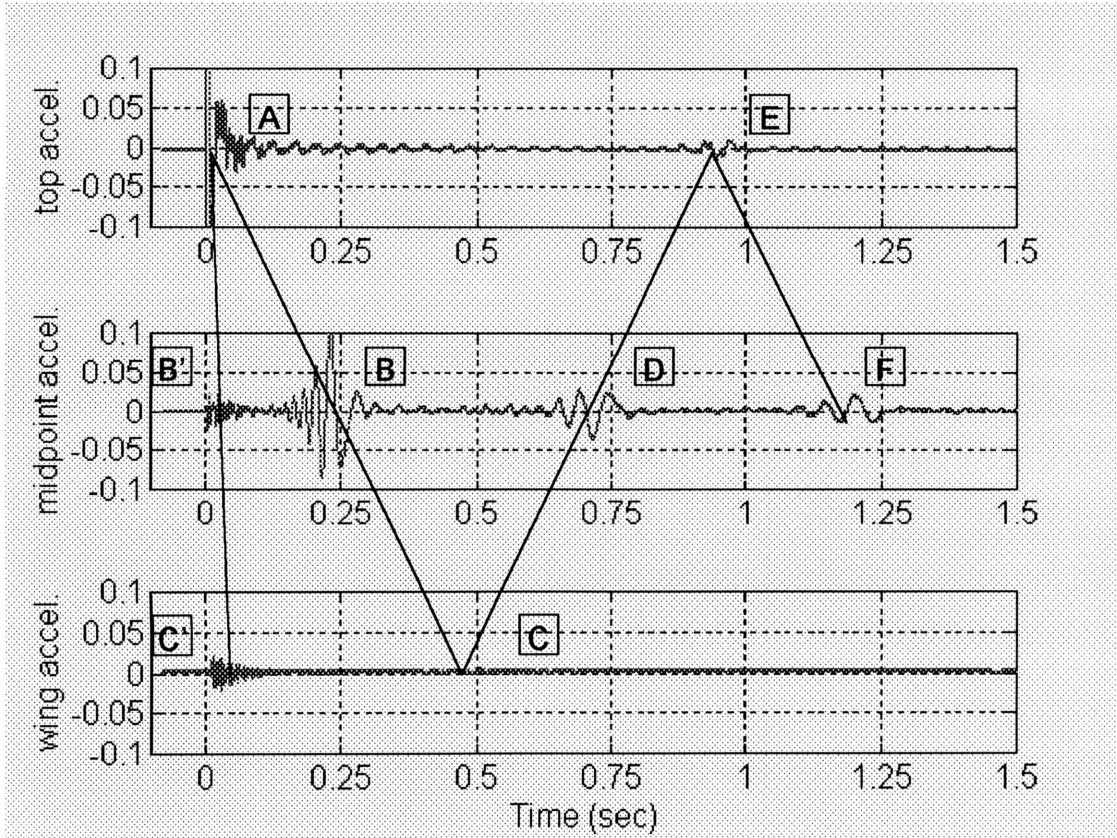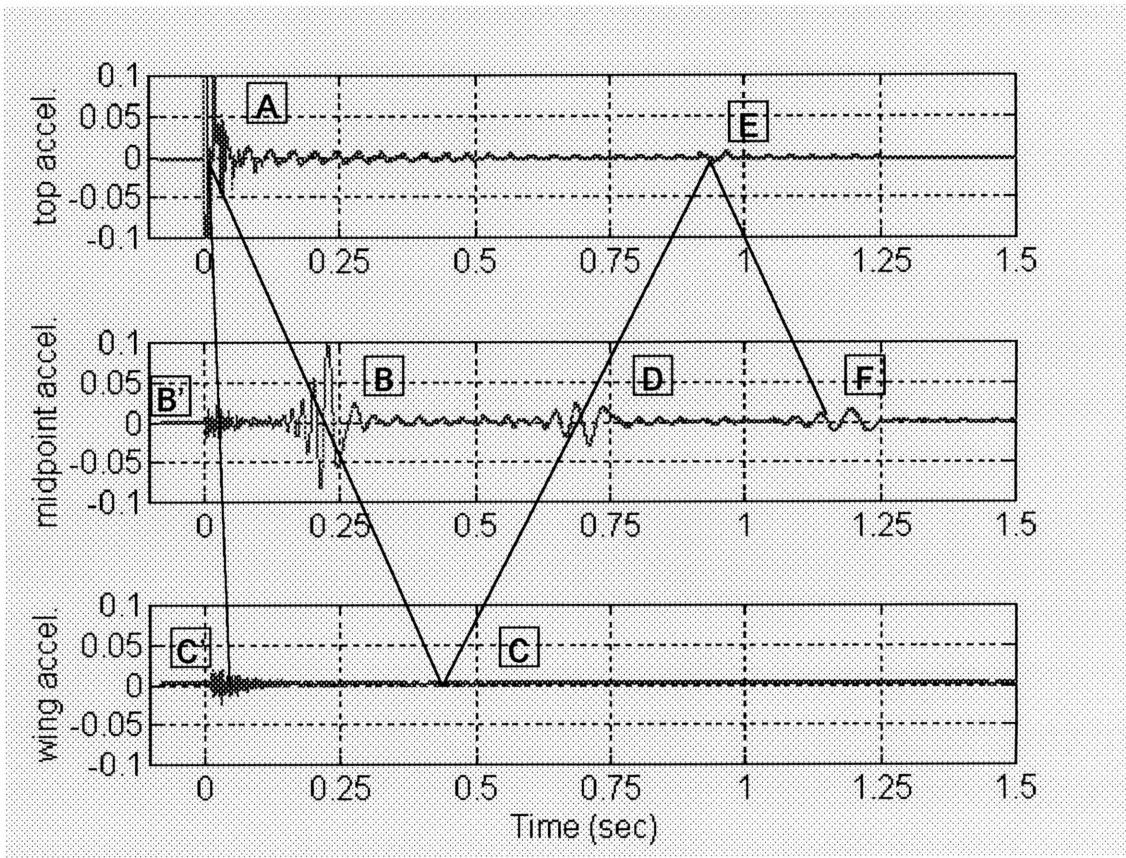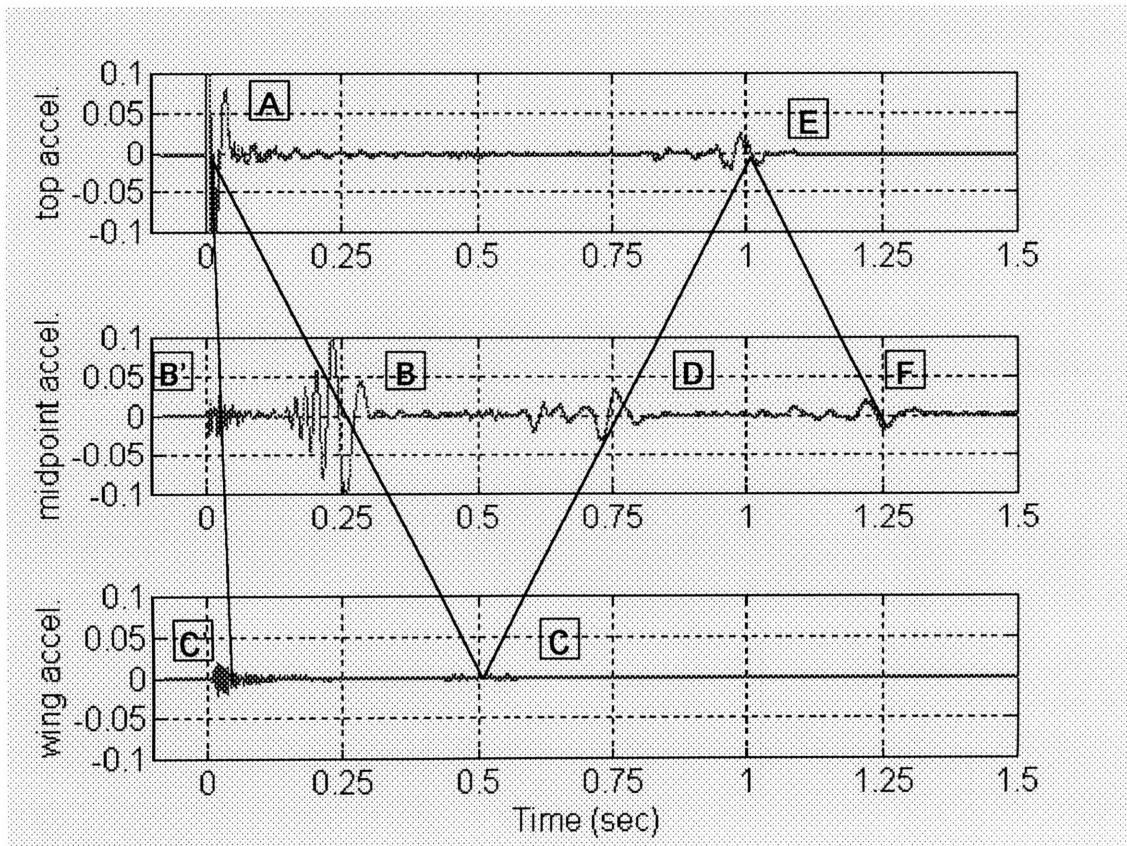

Figure 15: Damped response, stairway test

Figure 16: Overdamped response, stairway test

Figure 17: Undamped response, stairway test

At Sea

Description of setup

The assembly was to be towed from the stern of a pleasure craft, so it was necessary to develop a towing method in the absence of a winch or A-frame that would minimize risk to all equipment. A 4x6 timber was mounted athwartships on the stern cleats of the vessel. The upper termination was fastened to the underside of the cantilevered port end of the beam. To minimize bending stress in the timber during testing, an eye bolt was fastened to the extreme port end, and a spring line was run under tension to a forward cleat. A strip of small aluminum angle was fastened to the cable with cable ties just beneath the link to serve as an attachment point for accelerometers. A large protractor was affixed to the timber to measure scope angle. (See Figure 18.)
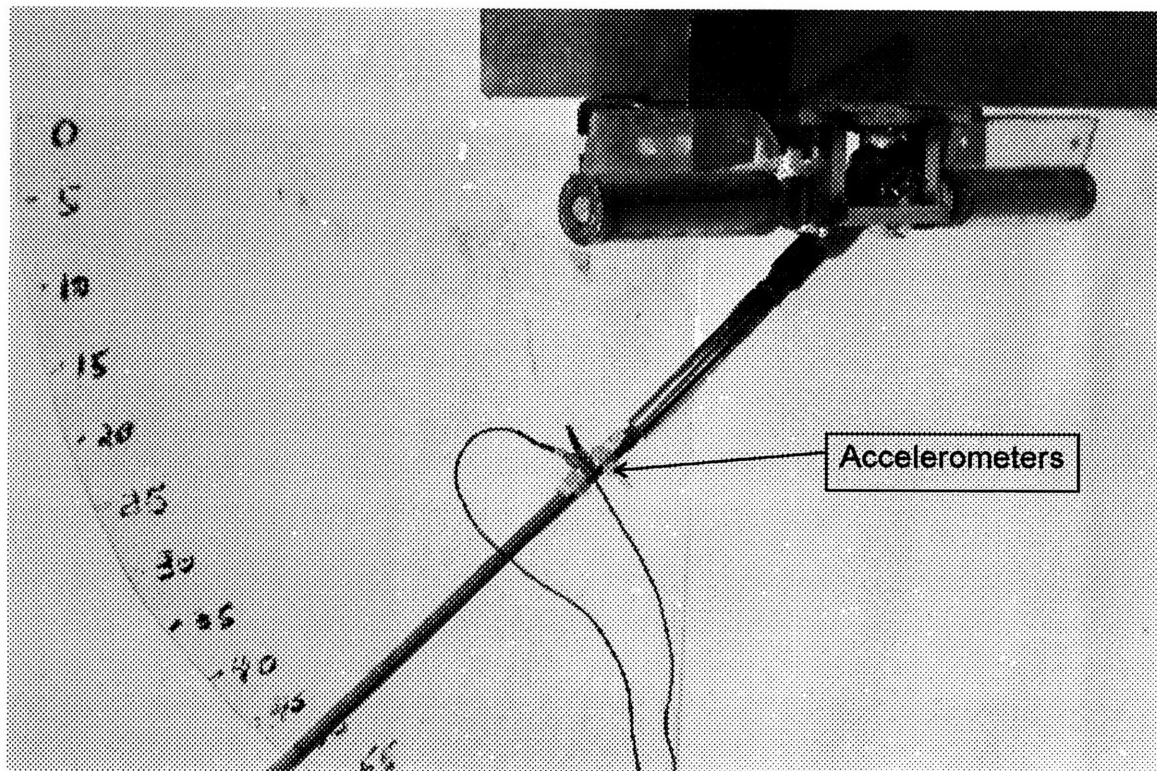

Figure 18: Upper termination, protractor, and accelerometers

Testing procedure

During the test, the vessel was run at several speeds up to six knots, and accelerometer data was taken with the dampers both engaged and disengaged. During the initial testing in the summer of 1994 a portable GPS (Global Positioning System) was used to determine speed over ground. RPM values from the engine were also recorded, and a conversion was developed to determine boat speed from engine RPM to be used during the second round of sea trials in the summer of 1995. The plot of frequency and tension versus boat speed is shown in Figure 19. PCB model A353B16 10 mV/g accelerometers were used to measure vibration, and a Hewlett Packard 3560A portable Fourier analyzer was used to capture and view the data.
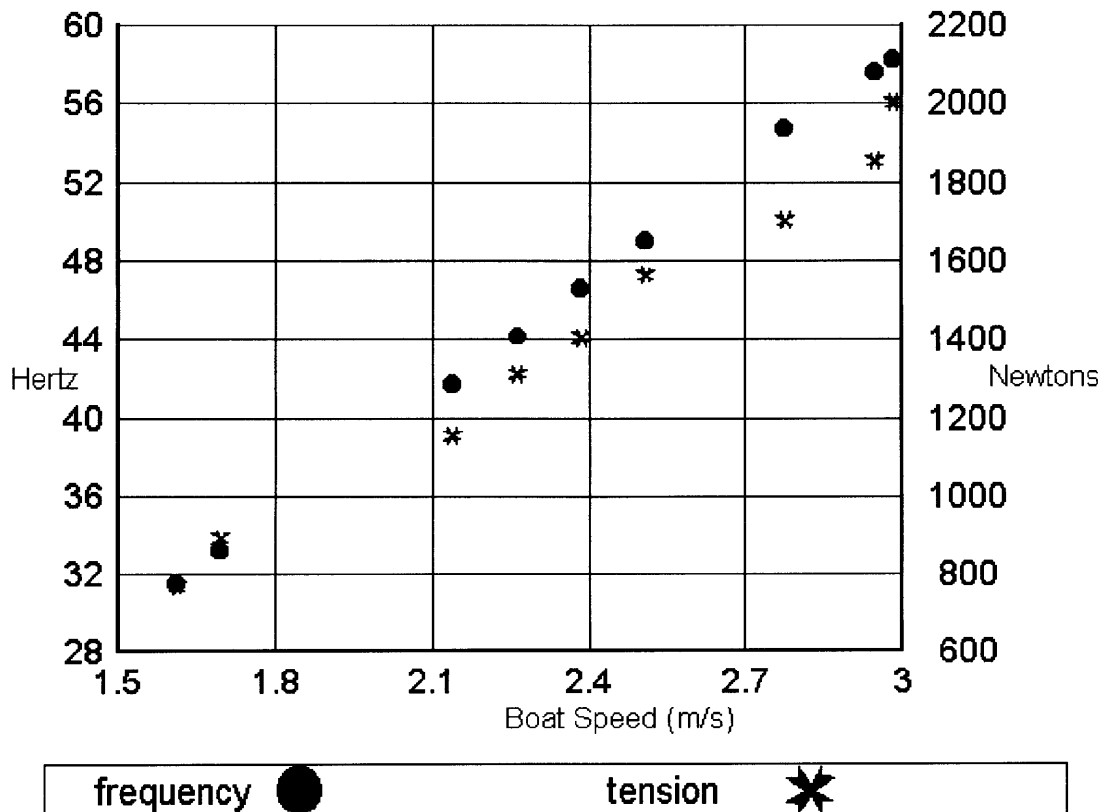

Figure 19: Frequency and tension vs. boat speed

Both autospectrum and time history data were taken during the tests, but the autospectra alone prove that the terminations were effective. Figure 20 shows a plot of two autospectra taken with dampers attached and unattached at the same boat speed. The two peaks are aligned, proving that the addition of the termination did not significantly alter the vortex-induced vibration frequencies of the system. However, the height of the peak corresponding to the damped test is almost sixty percent lower than the peak representing the undamped test. A similar result is true for all tested boat speeds and resultant vortex shedding frequencies.
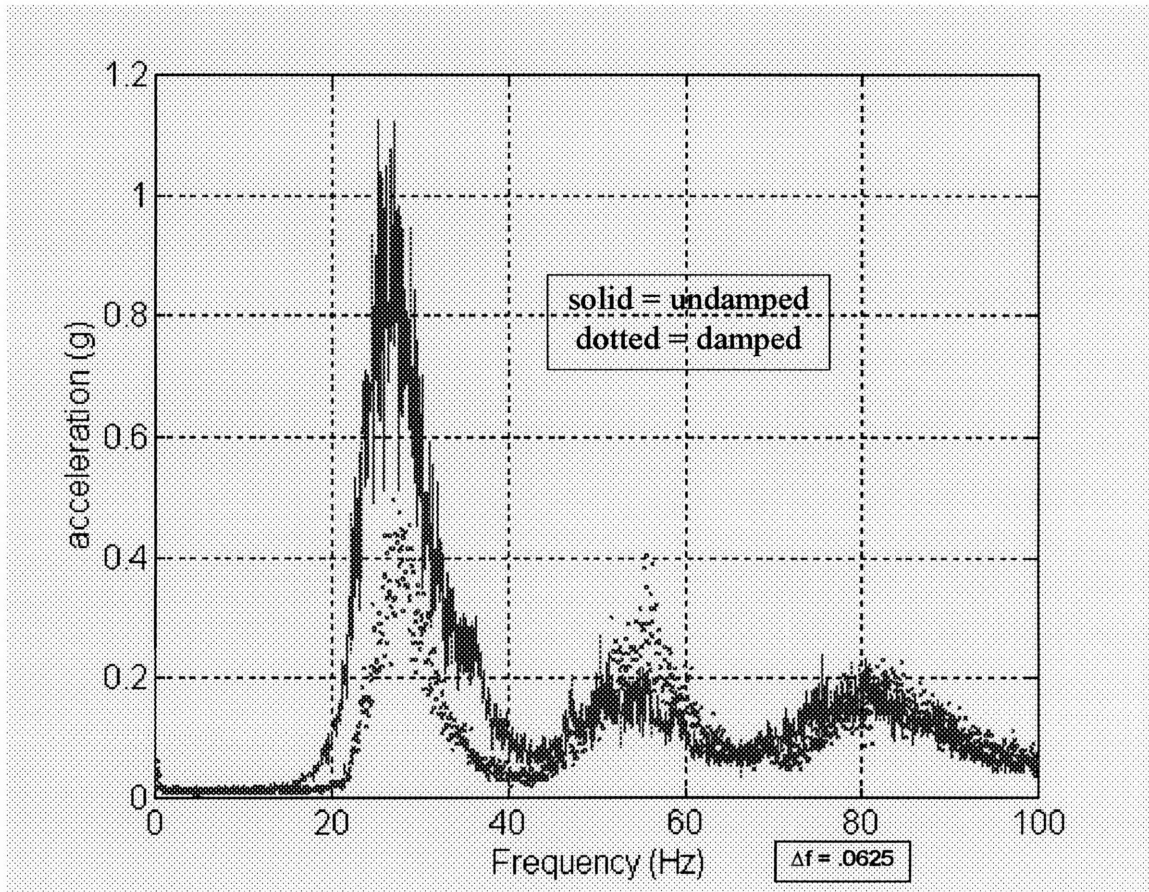
Figure 20: Acceleration of damped and undamped system at 26 Hz

Rms comparisons

To compare the sea trial results with the predictions of Dr. Li and Professor Vandiver, they must be in similar form. The predictions deal with

absorbed power, not reduction in acceleration. Since it is practically impossible with a constant vibration source to track a single wave through the termination and measure the absorption, the data must be analyzed in a slightly different fashion. The area under damped and undamped autospectrum plots for four characteristic boat speeds was estimated by integrating over the width of the principal response peak. The resulting mean square acceleration values were plotted over the nondimensionalized frequency $\overline{\omega}$. The data and calculations are displayed in Table 1.

freq. (Hz)	ω (rad/s)	T (N)	L_L (m)	I (kg*m^2)	$\overline{\omega}$	damped ms acc. (g^2)	undamped ms acc. (g^2)
26	163.3628	778.44	.16	.0018	.6269	55.3080	146.4274
43	270.177	1112.1	.16	.0018	.8675	380.6454	510.18
47	295.3097	1334.5	.16	.0018	.8656	426.0783	942.6725
57	358.1416	1556.9	.16	.0018	.9719	683.9873	1058.3

Table 1: Calculations for Figure 21

The area between the upper undamped curve and the lower damped curve represents the power absorbed by the system. It can easily be seen in Figure 21 that the power absorbed by the system is considerable when the dampers are attached and functioning.

24
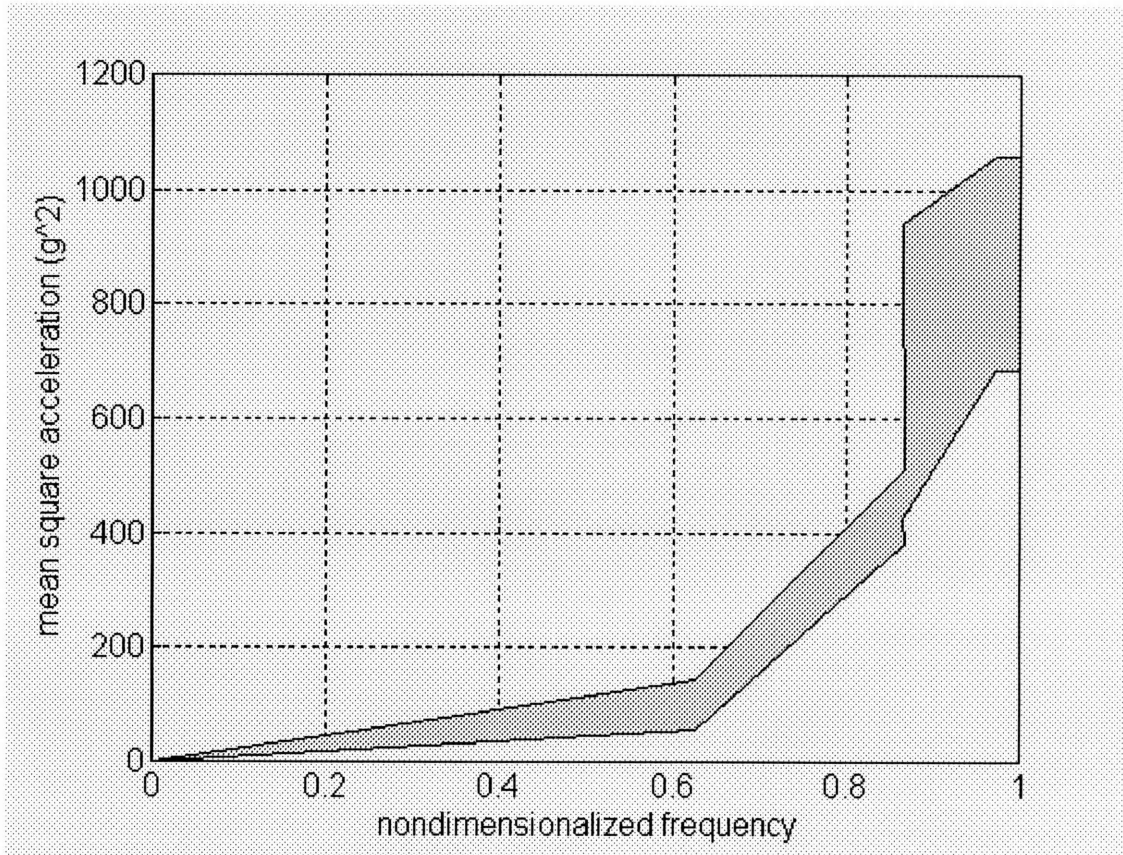
Figure 21: System power absorption vs. $\overline{\omega}$

Discussion

Performance of terminations

While the experimental results cannot be directly compared to the prediction curves created by Dr. Li and Prof. Vandiver, they do prove that a significant amount of vibration damping is occurring. The relationship between vibration and lift is a complex one, and it is unclear at this time exactly how a perfectly damped system of this type will look.

Possible improvements to apparatus

This design was created with an emphasis on simplicity and proof of concept. Of course before commercial application there should be some

attention paid to aesthetics, but other areas might be improved as well. In order to apply this technology to more diverse towing conditions, a design could be developed that self tunes to provide optimal damping at all times. A design of this type would be well suited to manufacturers of depressor wings, since the values that determine the damping envelopes are defined by these devices.

For example, the downward force on such a depressor wing in a current is defined as

$$T = w + \frac{1}{2}\rho_{SW}C_LSV^2 \tag{19}$$

where w is the weight of the fin in seawater, ρ_{SW} is the density of seawater, C_L is the lift coefficient of the fin, S is the planform area of the fin, and V is the current velocity. Since V-fins generate downward lift many times their own weight, this equation can be approximated as

$$T \cong \frac{1}{2}\rho_{SW}C_LSV^2 \tag{20}$$

This result is substituted into Equation 12 which defines the optimum operating frequency of the system, leaving

$$\Omega = \sqrt{\frac{TL_L}{I}} \cong \sqrt{\frac{\rho_{SW}C_LSV^2L_L}{2I}} \tag{21}$$

The optimal operating frequency Ω is set equal to the vortex shedding frequency detailed in Equation 1, producing

$$\frac{S_tV}{d} \cong \sqrt{\frac{\rho_{SW}C_LSV^2L_L}{2I}} \tag{22}$$

which simplifies to

$$d \cong S_t\sqrt{\frac{2I}{\rho_{SW}C_LSL_L}} \tag{23}$$

This equation is not a function of velocity, and therefore defines the correct cable diameter for a given V-fin and termination to construct a self tuning system.

However, the dampers must also be self tuning. Substituting Equation 20 into Equation 13 yields

$$R_\theta = L_L{}^2 \sqrt{T\rho_C} \cong L_L{}^2 V \sqrt{\frac{\rho_{SW} C_L S \rho_C}{2}} \qquad (24)$$

(It is important to note that ρ_C is a linear density and ρ_{SW} is a volumetric density.) Setting Equation 24 equal to Equation 16 gives

$$L_L{}^2 V \sqrt{\frac{\rho_{SW} C_L S \rho_C}{2}} \cong \frac{2\pi\mu_{eff} R_D{}^3 2 L_D}{h} \qquad (25)$$

which, using Equation 1, produces

$$\mu_{eff} \cong f \frac{dh L_L{}^2}{2\pi R_D{}^3 L_D S_t} \sqrt{\frac{\rho_{SW} C_L S \rho_C}{2}} \qquad (26)$$

This equation proves that in order to construct self tuning dampers of this type, the viscosity of the damper fluid must be linear with frequency. Equation 17 shows that the viscosity of the fluid used in this study was inversely proportional to frequency. As a result, the system was only optimally damped near one frequency.

Other applications of concept

This type of motile application alleviates just one manifestation of Vortex Induced Vibration. However, these terminations may be used in any scenario in which water moves past a slender cylinder. In the oceanographic arena, moorings commonly fit this description. Whether the employment is one as mundane as a marina mooring ball in tidal flow or as technological and fragile as a string of current meters or hydrophones in the Gulf Stream, VIV is a potentially destructive yet amendable problem.

Other damping materials may be used in these cases. Flexible silicone epoxies were tested for use in this particular experiment, but were found to have inadequate damping properties for higher cable tensions. These would be perfectly suited, however, to a situation with a lighter cable and/or lower tension, such as a light mooring.

27

Testing of silicone epoxy

It was not readily feasible to test this silicone epoxy on the original test bench. The components needed to be mixed and then set in a watertight configuration to cure for twenty four hours. To accommodate these construction limitations, a new testing procedure was developed. Casts were made using modeling clay to plug the bottom openings of several steel pipes of varying length and radius. A 1.5 foot length of half inch diameter knurled steel rod was set inside each of these pipes and pressed slightly into the clay to secure them in a concentric manner.

Primer provided by Emerson and Cuming Co., the manufacturer of the epoxy, ensured adhesion of the cured gel to most surfaces. This was applied to the inner surface of the pipe as well as the section of the rod inside the pipe, and allowed to dry. The epoxy components were mixed according to the instructions, and then set inside a vacuum chamber for several minutes to eliminate bubbles entrained during mixing. Once the mixture had achieved full outgassing, it was poured into the pipes until they were full. Bits of clay were inserted at the top end to ensure concentric alignment of the rods. The assemblies were kept oriented vertically with the clay plug at the base and allowed to cure. Figure 22 illustrates this casting assembly.

The different sized pipes created different epoxy thicknesses and lengths in each case. Although it did not exactly model the excitation in situ, an impulse test was used to determine the damping factor and stiffness factor of each assembly. To increase the moment of inertia of the systems, a piece of aluminum channel was glued at its midpoint to the bottom of each rod forming a "T". In an effort to maintain continuity, the same piece of channel was used to test each assembly. A 10 mV/g accelerometer was glued to the endpoint of the piece of channel. The pipe end was fixed in a vise allowing the rod and channel to hang down. The channel was hit at its endpoint with a hammer causing the rod to oscillate axially. Figure 23 shows the test setup.
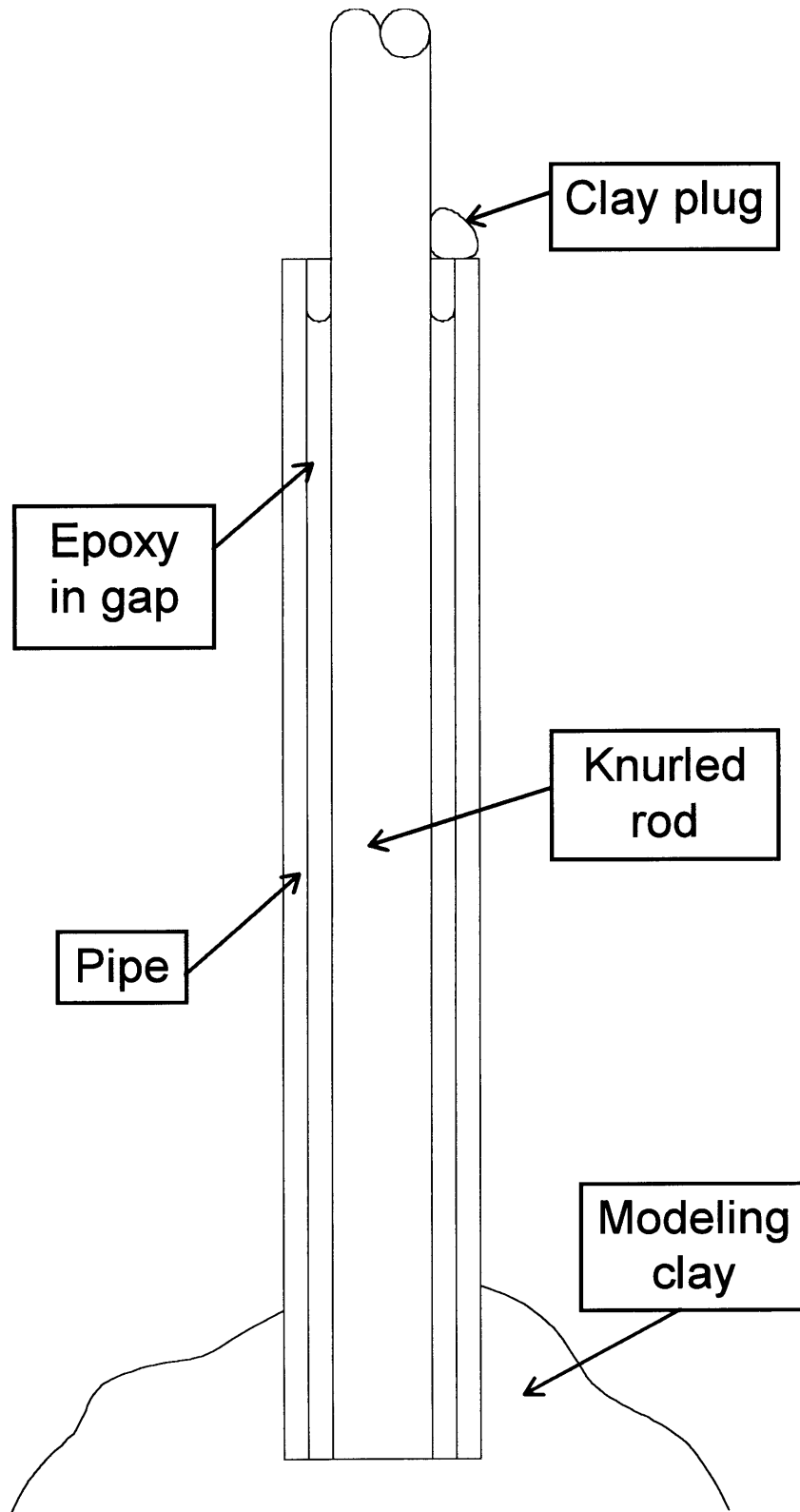
Figure 22: Casting assembly
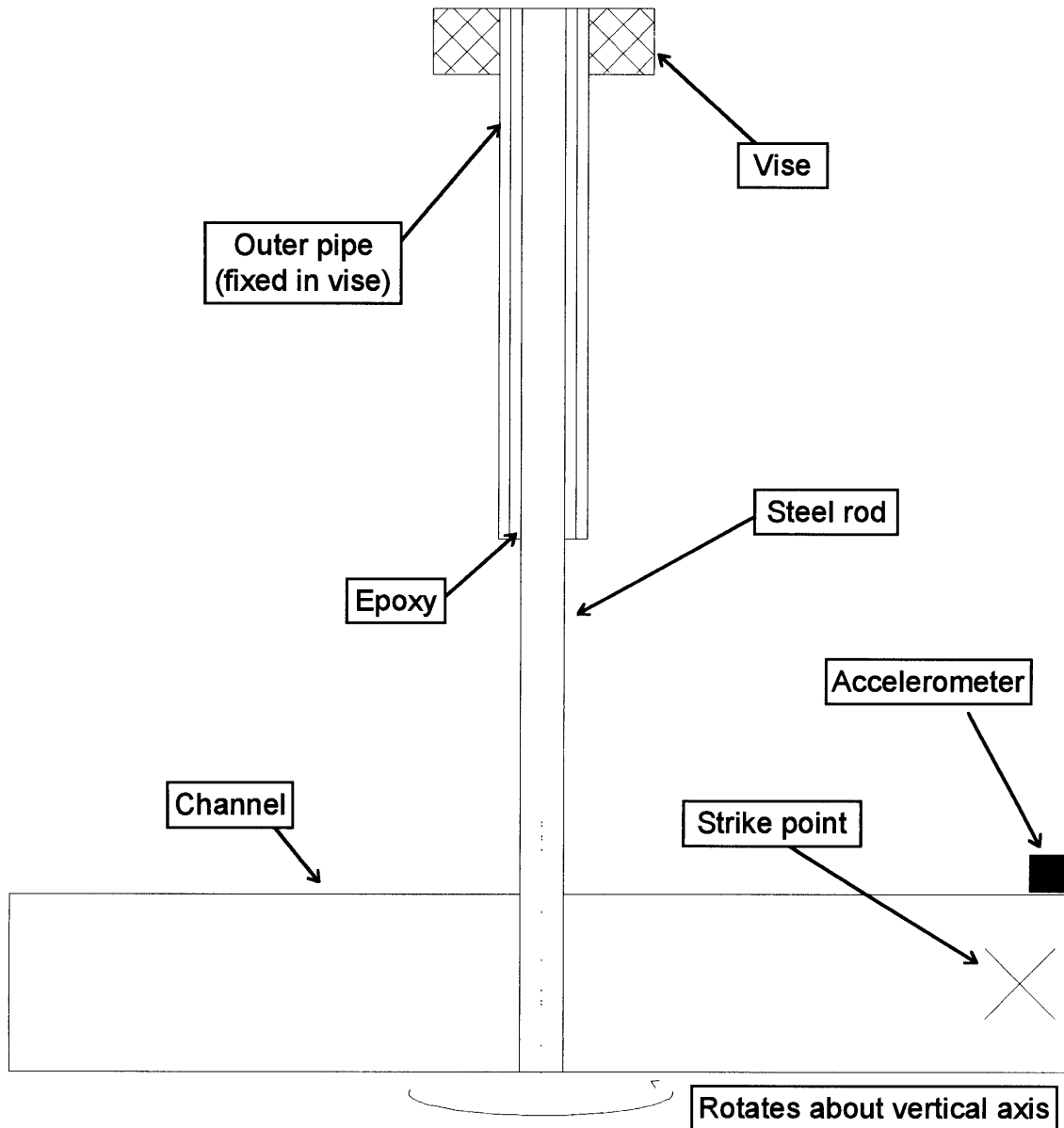
Figure 23: Solid damper test assembly

Time histories were taken in each case, as well as autospectra. The acceleration values of each peak in the time histories were determined, as well as the frequencies of the principal peaks in the autospectra. The log decrement, a parameter characterizing damping in a system, was calculated using the following equation

$$\delta = \frac{1}{m}\ln\left(\frac{x_1}{x_{m+1}}\right)$$

(27)

where m is an integer and m+1 is not greater than the number of recorded peaks, and x_m is the acceleration value of the mth peak as obtained from the time histories. The damping factor was then calculated using the equation

$$\zeta = \frac{\delta}{\sqrt{(2\pi)^2 + \delta^2}}$$

(28)

where δ is the log decrement. The natural frequency was then found using

$$\omega_n = \frac{\omega_d}{\sqrt{1-\zeta^2}}$$

(29)

where ω_d is the damped natural frequency as determined from the autospectra, and ζ is the damping factor. Once I the moment of inertia of the rod and channel was determined along the axis of the rod, it was used to calculate the system stiffness from the natural frequency using Equation 29

$$K_\theta = \omega_n^2 I$$

(30)

where ω_n is the undamped natural frequency and I is the moment of inertia of the system. Finally, the damping constant of the system was determined using the equation

$$R_\theta = 2\zeta\sqrt{K_\theta I}$$

(31)

where K_θ is the system stiffness constant in N·m/radian.

For example, an assembly with a damper L_D = 13 cm long, outer epoxy radius of R_o = 9.5 mm and a thickness of t = 3.175 mm yielded a log decrement of δ = .34946 and a damped natural frequency of ω_d = 33.772 rad/sec. Using Equation 28, ζ was found to be .05553. The undamped natural frequency was ω_n = 33.824 rad/sec from Equation 29. The moment of inertia about the rod axis was calculated to be I = 5.945 x 10^{-3} kg m^2 and plugged into equation 30 to find the system stiffness constant K_θ = 6.801 N·m/radian. Ultimately the damping constant was found to be R_θ = .02233 N·m·s/radian from Equation 31.

A model of the epoxy layer is shown in Figure 24. In order to determine the governing equations for such a damper using linear shear theory, it is important to make certain assumptions. Primarily, it must be assumed that the thickness of the epoxy layer is relatively small compared to the outer radius of the layer. If this can be done, it can be assumed that the shear force is equal to the shear modulus times the shear angle.
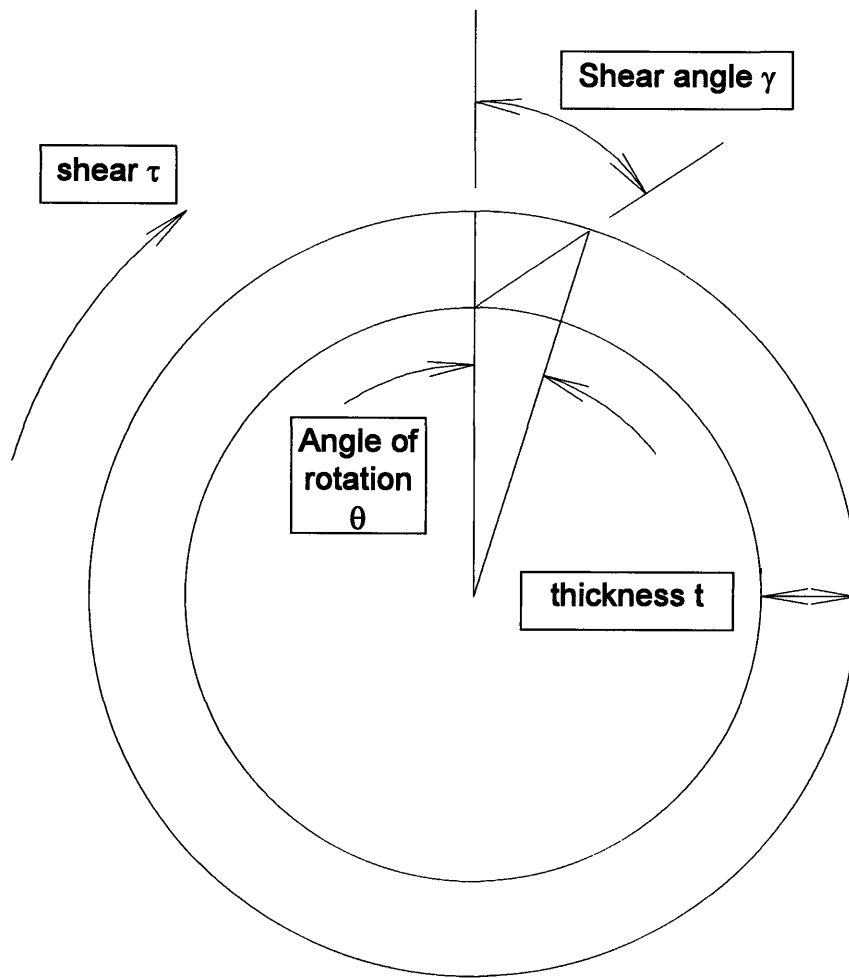
$$\tau = G\gamma \tag{32}$$

Figure 24: Diagram of epoxy layer

It can also be proven geometrically that when γ is small, the shear angle times the layer thickness equals the outer radius times the angle of rotation.

$$\gamma t = r_o \theta \qquad \text{or} \qquad \gamma = \frac{r_o \theta}{t} \qquad (33)$$

The applied torque is equal to the shear force times the outer surface area of the epoxy tube times the outer radius.

$$T = \tau 2\pi r_o^2 L_D \qquad \text{or} \qquad T = G\frac{r_o \theta}{t} 2\pi r_o^2 L_D \qquad (34)$$

At equilibrium, the applied torque is also equal to the spring constant times the angle of rotation.

$$K_\theta \theta = G\frac{r_o \theta}{t} 2\pi r_o^2 L_D \qquad \text{or} \qquad K_\theta = \frac{G 2\pi r_o^3 L_D}{t} \qquad (35)$$

Equation 35 relates the spring constant of such an apparatus simply to the geometry of the epoxy layer and the shear modulus. A similar equation for the damping constant can be found by substituting Equation 35 into Equation 31.

$$R_\theta = 2\zeta \sqrt{\frac{2\pi r_o^3 L_D G I}{t}} \qquad (36)$$

The numbers from the preceding example may be entered into either Equation 35 or 36 to find the shear modulus.

$$G = \frac{K_\theta t}{2\pi r_o^3 L_D} = 30833.5 \frac{N}{m^2 rad} \qquad (37)$$

A termination with two of these dampers would have R_θ = .03158 N·m·s/radian and K_θ = 13.602 N·m/radian. Assuming a link length of .16 meters, by Equation 13 this termination would have an input impedance of 1.23 N/m/sec. For example, the system would be optimally damped for a cable with a tension of 25 lb (or 111.2 N) and a linear density of .014 kg/m. Many commercially available Kevlar cables are made in this linear density range. Assuming a link moment of inertia of .0018 kg/m^2, by Equation 6 the system would be optimally tuned to a frequency of 21 Hz. Assuming a 55 ft (16.764 m) cable, by Equation 2 this frequency would coincide with the cable's 8th mode.